

Charge-State-Enhanced Ion Sputtering of Metallic Gold Nanoislands

Gabriel L. Szabo,* Benedykt R. Jany, Helmut Muckenhuber, Anna Niggas, Markus Lehner, Arkadiusz Janas, Paul S. Szabo, Ziyang Gan, Antony George, Andrey Turchanin, Franciszek Krok, and Richard A. Wilhelm*

Experimental results on the charge-state-dependent sputtering of metallic gold nanoislands are presented. Irradiations with slow highly charged ions of metallic targets were previously considered to show no charge state dependent effects on ion-induced material modification, since these materials possess enough free electrons to dissipate the deposited potential energy before electron-phonon coupling can set in. By reducing the size of the target material down to the nanometer regime and thus enabling a geometric energy confinement, a possibility is demonstrated to erode metallic surfaces by charge state related effects in contrast to regular kinetic sputtering.

1. Introduction

The engineering of material properties on the nanoscale is used in a plethora of technological applications ranging from cleaning and smoothing in surface science^[1] to machining lithography masks with focused ion beams for industrial use.^[2] When ions are used as tools, one utilizes the momentum of an incoming heavy ion in the keV energy regime to trigger collisional motion of surface atoms in order to drive erosion or

mixing processes. However, heavy ions obtain another distinct property which is often overlooked when considering tailored material machining - a changing charge state.^[3] Ions initially prepared in high charge states carry a potential energy, given by the sum of the binding energy of all missing electrons, in the order of several 10 keV.^[4] It was recently shown that the release of the potential energy leads to a gentle carving of material in a layer-by-layer fashion, because the energy transfer is very rapid and consequently limited to the first material monolayer(s).^[5,6] Material

damage by the ion neutralization is driven by electronic excitations triggered through the charge exchange.^[7] Naturally, this makes insulators and semi-conductors more prone to modifications by slow highly charged ions (HCI).^[8–12] Metallic surfaces have not unambiguously shown a susceptibility to potential energy deposition as high as 40 keV per incoming ion,^[13,14] even in the case of freestanding two-dimensional graphene.^[15] It is assumed that the intrinsically high charge carrier mobility in metals dissipates electronic excitations before a coupled atomic motion can set in.

One can, however, restrict the energy dissipation by introducing a geometrical energy confinement in isolated metallic nanoislands. Such solid nano-droplets have a large potential to be used for novel applications in nano-electronic devices such as 2D-transistors,^[16] where they are designated to contribute to low-power applications^[17] that could be substantial to counteract the increasing energy demand in integrated circuit devices. Recent studies on singly-charged low energy ions with nano-rods and -cubes showed interesting, yet largely unexplored effects with regards to erosion and ion channeling.^[18,19] In this study, we irradiate gold nanoislands grown on a MoS₂ monolayer^[20,21] with single slow highly charged xenon ions. On a MoS₂ monolayer substrate the gold nanoislands are bound via van-der-Waals forces only,^[21] which leads to a reduced thermal conductivity^[22] and electronic coupling.^[6] This increases the possibility to confine the potential energy in the island, presenting an ideal experimental system to study the coupling of electronic excitations to lattice-atom motion. We observe a reduction of the nanoislands' height as a result of individual HCI impacts by performing atomic force microscopy (AFM) measurements before and after irradiation. Additional correlated scanning electron microscopy (SEM) imaging reveals that smaller islands, not detectable with our AFM, even vanished

G. L. Szabo, H. Muckenhuber, A. Niggas, M. Lehner, R. A. Wilhelm
TU Wien

Institute of Applied Physics
1040 Vienna, Austria

E-mail: gszabo@iap.tuwien.ac.at; wilhelm@iap.tuwien.ac.at

B. R. Jany, A. Janas, F. Krok

Marian Smoluchowski Institute of Physics

Faculty of Physics, Astronomy and Applied Computer Science

Jagiellonian University

Lojasiewicza 11, 30348 Kraków, Poland

P. S. Szabo

University of California

Space Sciences Laboratory


Berkeley 94720, USA

Z. Gan, A. George, A. Turchanin

Friedrich Schiller University Jena

Institute of Physical Chemistry

07743 Jena, Germany

 The ORCID identification number(s) for the author(s) of this article can be found under <https://doi.org/10.1002/smll.202207263>.

© 2023 The Authors. Small published by Wiley-VCH GmbH. This is an open access article under the terms of the Creative Commons Attribution License, which permits use, distribution and reproduction in any medium, provided the original work is properly cited.

DOI: 10.1002/smll.202207263

after irradiation. A clear charge state dependence on the erosion is observed. Our work strongly indicates that the charge state of the incoming ion and its associated potential energy is the driving force in the erosion process of geometrically confined metallic objects. Our study therefore underpins our understanding of HCI-related nanometric surface modification processes and introduces a way to manipulate surface quantum dots post-growth without affecting the interface between the substrate and the dot.

2. Results

2.1. Charge Dependent Height Loss

To investigate a potential energy dependent erosion of metallic nanoparticles, gold nanoislands were irradiated with Xe^{q+} ($q = 1, 18, 25, 32, 40$). To analyse the height of the nanoislands, measurements were performed with AFM before and after irradiation. The main graph in **Figure 1** shows the height loss of the nanoislands as function of the potential energy of the HCI, with an increasing erosion yield with increasing charge state.

It is clearly seen that the change of the height is dependent on the potential energy deposited in nanoislands. The graph is surrounded by histograms according to the different charge states, where the blue histograms resemble the height distribution before and the orange histograms after irradiation. For Xe^{1+} and Xe^{25+} we observe bi-modal height distributions, which are a result of different growth modes of the Au islands close to the MoS_2 edges and in the center. In some cases, that is, on

some monolayers a higher density of smaller islands is found than on other monolayers. In our study smaller islands are less likely to be hit by an HCI and so we exclude them in the subsequent analysis, but show a second data point for Xe^{25+} for comparison (grey). In **Figure 1** one can see that the irradiation with Xe^{1+} induces no change of the size of the nanoislands, indicating a threshold for the potential energy (or charge state), above which alteration of the nanoislands is possible. This also means that the kinetic energy transfer of the impinging particle alone (180 keV) does not suffice to alter the height of the gold nanoislands in a detectable manner (the potential energy of Xe^{1+} of 11 eV can be neglected). Note that we applied low fluences such that each island is hit not more than once.

2.2. Correlative Microscopy

To highlight that the observed height loss also correlates to the islands' initial volume, the irradiation with Xe^{25+} is presented in more detail. We used the exact same spots on the samples for further analysis and performed a 1:1 comparison of the same islands before and after irradiation. This means that the height differences are determined for each nanoisland individually, with at least 100 islands measured for sufficient statistics. In contrast to previous experiments on HCI-induced surface erosion, here we do not rely solely on statistical averages of structure sizes.

To obtain accurate dimensions of the gold nanoislands, the samples were examined with AFM and SEM, since the AFM measurements yield the true physical height (which cannot be

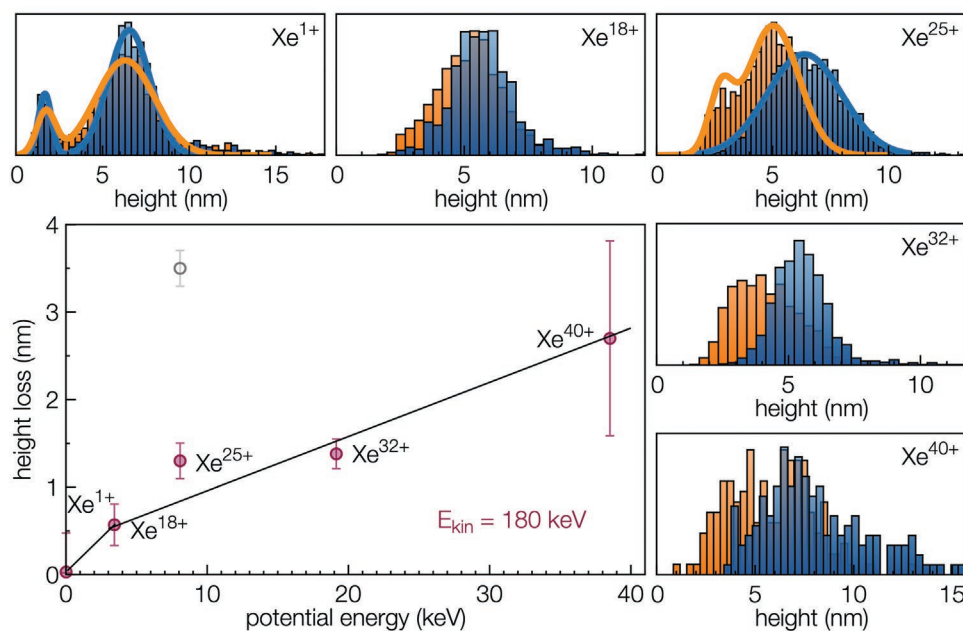


Figure 1. This graph shows the height change of the gold nanoislands after irradiation with Xe^{q+} ($q = 1, 18, 25, 32, 40$), with the histograms surrounding the graph showing the height distributions for each charge state before (blue) and after (orange) irradiation. In the graph a clear charge-state dependence of the height loss is visible. The higher the charge state of the impinging ion is, the higher the change in height after irradiation. The error bars for the height loss represent the error of the mean value (in this case $\frac{3\sigma}{\sqrt{N}}$; N : number of islands; σ : standard deviation). Bi-modal distributions are observed for Xe^{1+} and Xe^{25+} , which is a result of different height distributions due to the growth process before irradiation and due to the fact that not all islands measured are actually hit by a HCI.

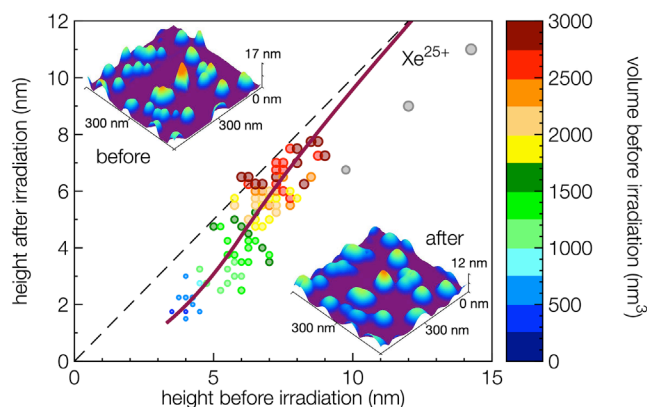


Figure 2. Height of the gold nanoislands compared before and after irradiation with Xe^{25+} . 101 individual islands were investigated. The color-bar and the size of the dots indicate the volume of the nanoislands before irradiation to highlight the different susceptibility for a height change regarding the initial volume. It can be seen that the lower the volume the higher the change due to the ion impact. The dashed line indicates no height change and the solid line is to guide the eye. The three grey points are excluded from the analysis due to their largely different aspect ratio (height vs. area), which can be seen in more detail in Figure S1 (Supporting Information). Inserted are also 3D-images with the same scale from AFM of the same area that show the reduction of the nanoislands' height.

obtained with SEM) and the SEM measurements yield a chemical composition contrast and a higher resolution regarding the edge length of the nanoislands which is obscured due to tip geometry and convolution artefacts present in AFM.^[23,24] Also for both AFM and SEM the exact same islands were compared (correlative microscopy), where it was found that the nanoislands measured with AFM appear approximately 1.79 times larger in lateral elongation.

The AFM images were then analysed to study the height and volume of the nanoislands, where for the latter the lateral lengths were connected with found factor of 1.79. In **Figure 2** the height change due to the irradiation with Xe^{25+} is related to the islands' volume prior to irradiation. It can be seen that, in general, bigger islands experience a smaller change in height than smaller islands. A visible change in height loss was observed for volumes (before irradiation) of approximately 1600 nm^3 (see **Figure 2** with very few exceptions). This can be seen as a drop in the solid red curve that starts at islands that are colored dark green (initial island volume $\approx 1600 \text{ nm}^3$). Note that it could also be possible that only parts of the islands are affected by the potential energy (e.g., the sharp edges of the islands) or a larger island only partially melts.

2.3. Melting and Evaporation of Nanoislands

Additional effects, besides the most prominent height reduction, were observed for the irradiation with Xe^{40+} . The first one is the vanishing of very small islands after irradiation, which can be seen in **Figure 3a** and **b**, where the missing islands are marked with red circles. The islands' initial volume prior to irradiation is estimated to be between $60\text{--}150 \text{ nm}^3$ for the vanishing islands, which is important for further investigations

on confinement of the potential energy in the islands. Those small islands were only observed with SEM measurements, because their size is too small for a detection with an AFM. The second effect observed after irradiation with Xe^{40+} is shown in **Figure 3c,d**, where a wetting around of some of the nanoislands can be seen. This was observed for both AFM and SEM measurements indicating that also bigger islands are affected by HCIs. The wetting behaviour was only found in immediate proximity of nanoislands.

Schweska et al.^[6] and Hopster et al.^[25] have recently reported that freestanding MoS_2 and MoS_2 substrate, respectively, are susceptible to damage induced by HCIs. However, due to the dense growth of the gold nanoislands on the substrate and a reported pore diameter in MoS_2 of approximately 4 nm , we could not resolve damage with AFM and SEM measurements. The residuals around the nanoislands were investigated with SEM in a low energy (5 keV) BSE (back-scattered electrons) mode, where the strong chemical composition contrast between the wetting layer (purple) and the MoS_2 background (black) lets us assume that the material is gold.

3. Discussion

To better understand the combination of processes that take place when metallic nanoclusters are irradiated, both the potential energy effect and the kinetic energy effect are discussed separately and subsequently combined in the following chapters.

3.1. Potential Energy Confinement

To describe the observed evaporation and partial melting in **Figure 3**, the heat of fusion for gold of $12.55 \text{ kJ mol}^{-1}$ ($120 \text{ meV atom}^{-1}$), the potential energy of $\text{Xe}^{25+} \approx 8000 \text{ eV}$ and the atomic volume of gold with $58.9 \text{ atoms nm}^{-3}$ are considered. With this, we can estimate an approximate threshold for melting induced by the HCI. Assuming a $80 \pm 10\%$ conversion of the potential energy into heating,^[26] islands below $\approx 1000 \text{ nm}^3$ should melt completely. In **Figure 4** the factor^[27,28]

$$k = \frac{E_{\text{elec}}^{\text{dep}}}{E_{\text{melting}}} \quad (1)$$

is shown for a nanoisland with a height of 6 nm , where $E_{\text{elec}}^{\text{dep}}$ resembles the deposited energy (into the electronic sub-system of the material) which is $\approx 80 \pm 10\%$ of the initial potential energy of the impinging HCI and E_{melting} is the energy needed to melt the entire island. For a perfect confinement, and hence a complete melting would occur at $k \geq 1$. In ^[27,28] the electronic excitation induced by swift heavy ions in a 3D gold cluster was investigated. In these studies, it was estimated that $k \approx 1.9$ can be approximated, which was, however, for a gold nanoparticle embedded in a SiO_2 matrix. Contrary to that, in our study the gold nanoislands are only in contact with the surrounding environment via their contact plane. Additionally, the gold islands are only bound via van-der-Waals forces, which were found to be low ^[22] and have thermal boundary conductance up to 10x lower than stronger bound contacts,^[29] strengthening the

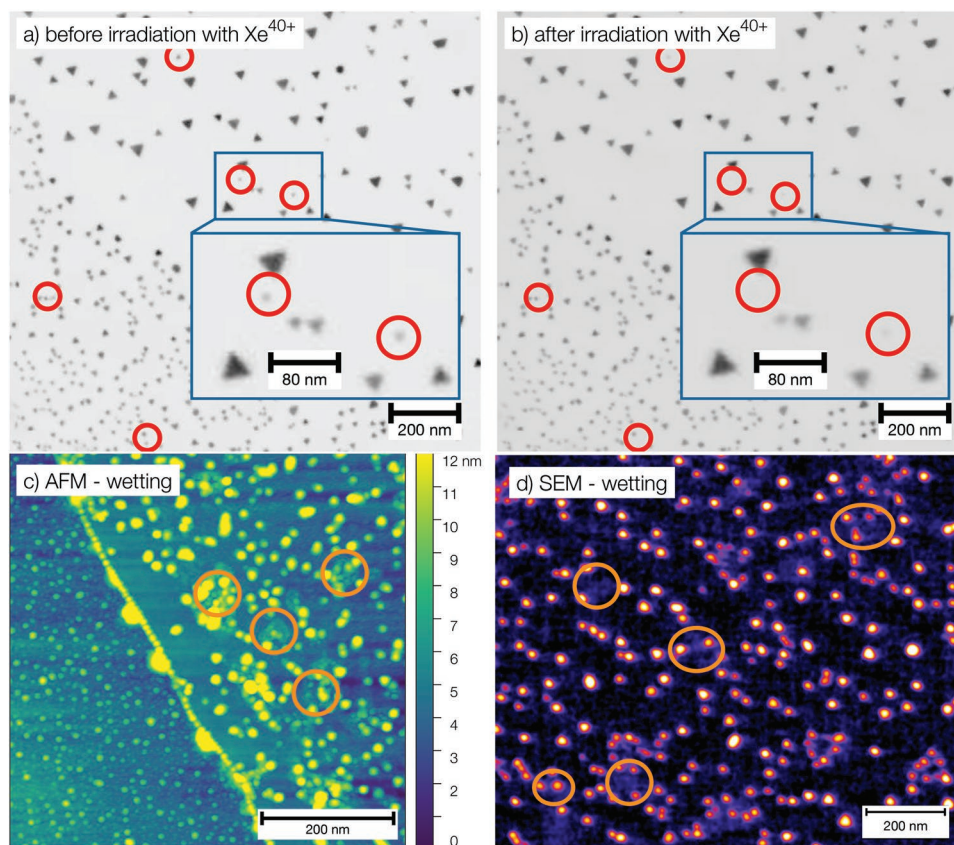


Figure 3. In a,b) SEM images of the same spot are shown before and after irradiation illustrating the vanishing of smaller islands. In c) an AFM image and in d) a SEM BSE (back-scattered electrons) image is shown where a wetting layer is visible close to nanoislands after irradiation with Xe^{40+} . The red circles in (a,b) mark the nanoislands that are molten or evaporated due to irradiation with Xe^{40+} . The volume of the missing islands is estimated with approximately $60\text{--}150\text{ nm}^3$. Visible wetting effects, only found after irradiation, are marked with orange circles in (c,d) in both images (lighter contrast in AFM and darker contrast in SEM). Due to the strong chemical contrast in SEM BSE between the MoS_2 and the molten residuals around the islands it can be assumed that the material is actually gold. Note that for (a,b) the contrast of the images was inverted for a clearer representation.

assumption that the deposited energy mainly stays confined within the nanoislands. The thermal boundary conductance between gold and monolayered MoS_2 was found to be very low at $0.44 \pm 0.07\text{ pWnm}^{-2}\text{K}^{-1}$.^[30] Staechelin et al.^[31] have observed that scattering of electrons on the surface of poly-crystalline gold nanoparticles can be neglected, that is, that “hot” electrons stay confined long enough within the nanoparticle for electron-phonon coupling to set in. Those findings indicate that the k-factor for our study should be very close to 1.

With this, Figure 4 indicates that predominantly the irradiations with Xe^{40+} should show complete melting or evaporation of smaller islands (considering that the majority of the measured islands have a lateral length between 15 and 40 nm). Smaller islands should melt completely what may explain the SEM measurements after irradiation with Xe^{40+} in Figure 3a,b. There, the islands are estimated with a volume of approximately $60\text{--}150\text{ nm}^3$, which is significantly below the melting threshold.

3.2. Kinetic Energy Effect

To estimate the effect of kinetic sputtering without any charge state effects alone, we used the SDTrimSP-3D-code,^[32–34] which

allows the simulation of sputtering of 3D-objects. Results of a simulation can be seen in Figure S2 (Supporting Information), where two different sizes of gold nanoislands were simulated. The size dependence of the kinetic sputtering is small, while there exists an enhanced sputtering from the island edges as a result of the additional side surface. For this simulation the sputtering of Mo and S was not investigated. Recent studies^[35–37] also suggest that nano-particles are more susceptible to increased sputtering yields when the penetration depth of the particle is in the same range as the lateral dimensions of the nano-particle. A more detailed description of the simulated nanoisland and how the sputtering yield is calculated can be found in Figures S3 and S4 (Supporting Information).

To emphasize the vanishing influence of kinetic sputtering even more, let us discuss the experiments with individual Xe^{1+} ions in more detail, while a possible enhancement of the kinetic energy deposition by the charge state directly is discussed below. It should be mentioned that for the current experiments, fluences were chosen so low that only single hits per island are statistically possible, excluding dynamic effects like shape change due to high fluences. Earlier experiments conducted by Donnelly and Birtcher^[14,38,39] found small craters on flat gold surfaces after irradiating the sample with single Xe^{1+} ions with

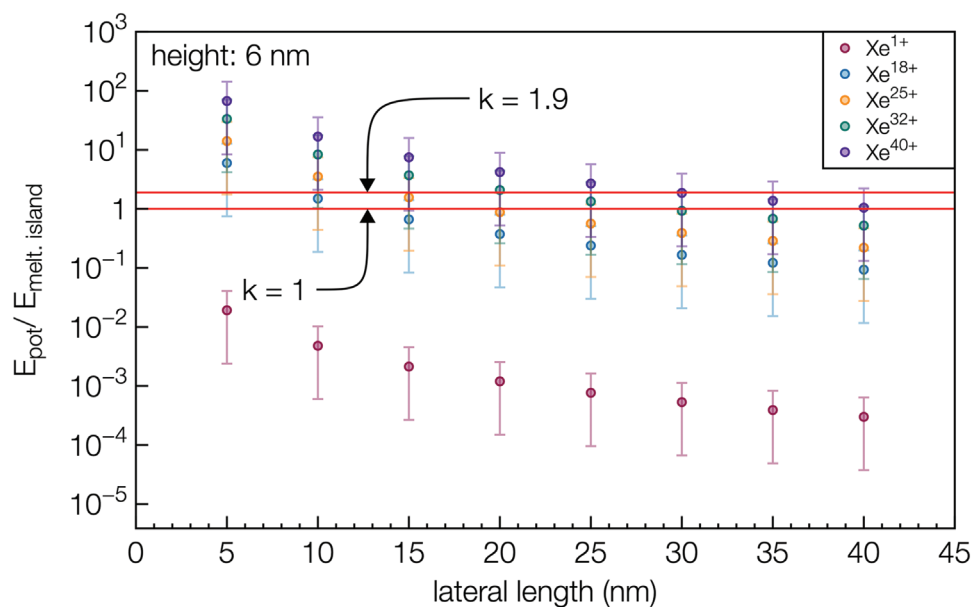


Figure 4. Calculated ratio of potential energy deposited in the island versus the energy necessary to melt an entire island with a height of 6 nm, dependent on different lateral lengths of the nanoisland. Note that the y-axis is logarithmic. Here, only 80% of the initial potential energy of the HCI is considered according to [26]. The different colors mark the charge states used in this work and the k-factor of 1.9 shows the upper limit for the confinement effect of nanoparticles that experience strong electronic excitations.^[27,28] The error bars mark an error of $\pm 10\%$ according to the findings in.^[26]

a kinetic energy of 200 keV. The observed erosion per ion was about 3500 atoms, which is below the detection limit for our nanoislands. Once an increased charge and additional potential energy is introduced, for example, 3.43 keV for Xe^{18+} , a significant change of the nanoislands' height can be observed after irradiation. The role of the ion charge state is two-fold, that is, it leads to a high potential energy, but also to an increased kinetic energy loss as a result of an increased scattering cross section. This was initially discussed by Biersack.^[40] He found that Xe^{40+} has a strongly increased nuclear stopping force for kinetic energies below 300 keV due to a high initial charge state. Subsequent experiments indicated also a strong dependence of the charge state for energy loss in thin carbon foils.^[41] Similar experiments were performed by our group,^[42–44] followed by a theoretical model describing the charge state dependence of the nuclear stopping.^[45]

Based on previous findings on charge-state-enhanced kinetic sputtering the erosion yield from SDTrimSP may be increased by a factor of 5–8 and would then amount to approximately 200–350 atoms ion^{-1} . This alone would also not suffice to explain the significant height reduction as seen in Figure 1. Further, we did not observe the formation of craters presented in,^[13,14,38,46] which we link to the limited volume of the nanoislands. Instead of crater formation, where the width of the craters was assumed to be dependent on the potential energy, the ablation of several monolayers and wetting surrounding the irradiated area can be observed in our study.

3.3. Erosion Process

With both the kinetic and the potential energy contribution being discussed in detail, the energy deposition into the target

material is described in the following and is schematically shown in Figure 5: The HCI approaches the target's surface with a potential and kinetic energy. The interaction with the target electrons starts within 1–2 nm above the surface according to the classical-over-barrier-model.^[47] Immediately after the ion impact on the surface, the potential energy gets deposited initially within the first 1–3 monolayers^[48] in the vicinity of the impact point by exciting target electrons. Due to the limited volume of the nanoisland, the potential energy cannot dissipate at first, albeit the conducting properties of gold. A transfer to the substrate is also limited due to van-der-Waals-bonds exhibiting a weak interlayer conductance^[6] and due to the semi-conducting properties of MoS_2 . This leads to high energy confinement for a comparably long time (\leq ps). Additionally, the ion also carries a kinetic energy that gets deposited in the nanoislands via direct knock-on processes. Contrary to collisions with neutral atoms, a charge-state-enhanced nuclear stopping is present.^[40–43,45] Subsequently, dense collisional cascades at the surface are formed, leading to prompt sputtering of the target atoms and a substantial bond weakening of the remaining atoms. The combination of the deposited potential energy and the charge-state-enhanced kinetic energy loss posterior impact is stored in the gold nanoisland ultimately in the form of atomic motion (or heat). It leads to sputtering or melting of a significant part of the island. The result is an eroded island in conjunction with material outflow wetting the substrate.

4. Conclusion

In this study, we present a possibility to effectively erode and shape metallic nanoislands post growth. Contrary to recent studies, a clear indication for charge state effects on metallic

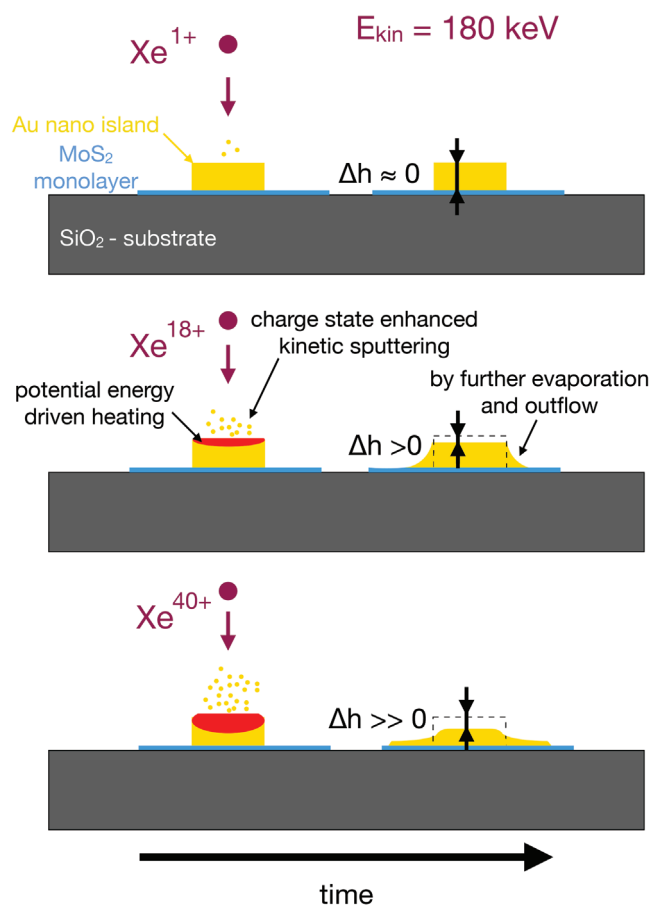


Figure 5. Schematic describing the surface erosion of the gold nanoislands dependent on the charge state of the impinging HCl, where Xe^{1+} induces no visible damage while with increasing charge state the height reduction of the nanoislands increases.

targets is present when reducing the material size down to the nanoscale. Our work therefore opens the possibility to increase the set of tools in nanotechnologies for post growth machining of nanometric quantum dots by adding the capacity of heavy ions in high charge states. Furthermore, our study helps to settle the open question about the susceptibility of metallic surfaces to HCl related material damage.

5. Experimental Section

Nanoislands Growth: All experiments discussed in this manuscript were performed on gold nanoislands (typical lateral size of 10–80 nm and an average height between 5–7 nm) on a monolayered MoS_2 substrate. The MoS_2 was grown on a substrate SiO_2 utilising chemical vapour deposition (CVD).^[20] The gold nanoislands grow as (111) orientated epitaxially on 2H- MoS_2 monolayers,^[21,49] which prevents clustering of the gold and induces a triangular shaped growth. For this growth process, the single layer MoS_2 crystals on SiO_2/Si were introduced into a UHV system with a base pressure of 10^{-10} mbar.^[20,49] The deposition of 1.5 ML (monolayers) of gold was performed by molecular beam epitaxy at 823 K substrate temperature with a rate of 0.12 ML min^{-1} , which was controlled by a quartz micro-balance. Following this procedure the sample was kept at the same temperature for 30 min before it was slowly cooled down to room temperature.

SEM Measurements: Later, to verify the growth of distinguishable gold nanoislands, measurements with a SEM Quanta 3D FEG by FEI were performed. The measurements were done in the BSE mode where the electron intensity is proportional to the atomic number Z , resulting in a chemical composition contrast with beam deceleration at 10 keV electron landing energy and without deceleration at 5 keV.

AFM Measurements: After verification with SEM, measurements were performed under ambient conditions using a tapping-mode AFM (Asylum Research Cypher Scanning Probe Microscope) showing an approximately 0.9 nm thick layer of MoS_2 (also visible with optical microscopy due to the different optical contrast of MoS_2 monolayers on 290 nm thick SiO_2 compared to multi-layered MoS_2) with nanoislands on top of it in the range of 5–7 nm. Super-sharp AFM probes were used for a better resolution (NanosensorsTM SSS-FM-20, Force constant $0.5\text{--}9.5 \text{ N m}^{-1}$) with a tip radius of curvature in the range of 2–5 nm. The AFM images were analysed with the software Gwyddion^[50] and by manually calculating the islands height: the substrate around the nanoisland was levelled to obtain a reference plane, from which the height of the nanoislands was deduced.

Irradiations: The irradiations of the gold nanoisland samples with charge states higher than 1 were performed at TU Wien using an electron beam ion source (Dresden EBIS-A from DREBIT GmbH, Germany), which is part of versatile setup to extract and utilize xenon ions with a charge state up to Xe^{44+} (for a detailed description of the setup see.^[51,52]) Xenon ions with charge states Xe^{q+} ($q = 18, 25, 32$, and 40) were generated with the ion beam setup. All ion species were accelerated to the same final kinetic energy of approximately 180 keV. The beam was shaped (with different apertures along the beam axis and electronic lenses) into a rectangular form with dimensions of $1 \times 2 \text{ mm}^2$ (which was controlled with a delay-line detector.^[53]) The fluence can be determined directly from the ion countrate which is obtained with the same detector.

Further irradiations with 180 keV Xe^{1+} ions were performed at the 500 keV ion-implanter located at the Ion Beam Center of the Helmholtz-Zentrum Dresden-Rossendorf, as singly charged ions with such a high kinetic energy cannot be produced at the setup at TU Wien. Adding an experiment with singly charged ions allows the comparison of a broad

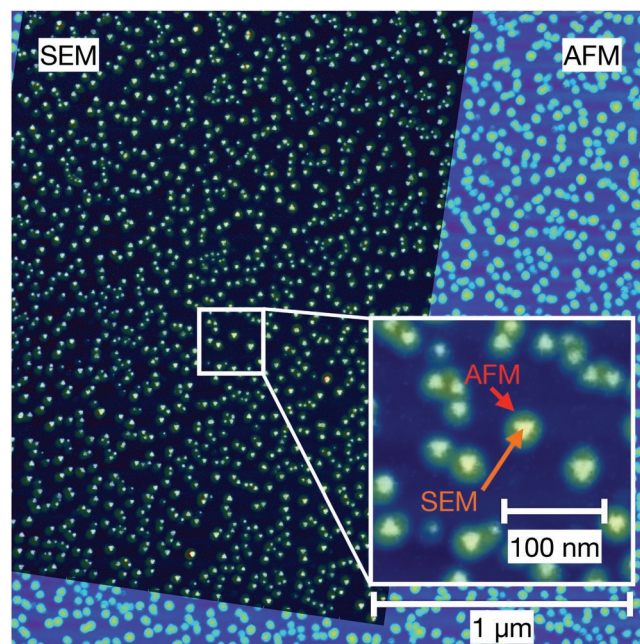


Figure 6. Comparison of an AFM image and a SEM image where the gold nanoislands are shown. The opacity for the SEM image was set to 75%, while for the insert it was set to 50% to highlight the different resolutions for the different imaging techniques.

range of charge states to single out the potential-energy-related effects for the manipulation of the Au islands.

Fluences: The samples were irradiated with different charge states and fluences. The irradiation with Xe^{1+} and Xe^{40+} were each conducted on different samples, while the irradiations for Xe^{18+} , Xe^{25+} and Xe^{32+} were performed on the same sample on different areas. To prevent irradiation with multiple charge states on the same spot, the sample was covered with an aperture that allowed only the irradiation of the intended area. In the following the fluences are listed for each charge state: 1×10^{11} ions cm^{-2} for Xe^{1+} , 7.5×10^9 ions cm^{-2} for Xe^{18+} , 7.5×10^9 ions cm^{-2} for Xe^{25+} , 5.1×10^9 ions cm^{-2} for Xe^{32+} and 1.06×10^{10} ions cm^{-2} for Xe^{40+} . The fluences are chosen such that each island can only be hit once by a single ion, that is, the probability for a double hit is vanishing. This fluences result to the following rate of hits: for Xe^{1+} approximately 71.3% of the islands were hit, for Xe^{18+} 53.6%, for Xe^{25+} 55%, for Xe^{32+} 36% and for Xe^{40+} 75.4%.

Analysis: After the irradiations the samples were analysed again with AFM under ambient conditions and with SEM under UHV conditions. A comparison between the AFM measurements and the SEM measurements can be seen in **Figure 6** where the exact same islands are shown before irradiation, measured with SEM and AFM. For the analysis between 160 and 2000 islands were measured on different MoS_2 monolayers. The errors are calculated as the error of the mean value $\frac{3\sigma}{\sqrt{N}}$, where N is the number of islands and σ is the standard deviation.

Supporting Information

Supporting Information is available from the Wiley Online Library or from the author.

Acknowledgements

This research was made possible by the Austrian Science Fund (FWF) (grant nos. Y 1174-N36, I 4914-N, and P 36264-N). P.S.S. acknowledges support from NASA's Solar System Research Virtual Institute (SSRVI) via the LEADER team, grant #80NSSC20M0060. Z.G., A.G., and A.T. thank the DFG support (grant TU 149/16-1). Parts of this research were carried out at IBC at the Helmholtz-Zentrum Dresden-Rossendorf e. V., a member of the Helmholtz Association. This research was supported in part by the Excellence Initiative - Research University Program at the Jagiellonian University in Krakow. The authors would like to thank U. Kentsch for assistance.

Conflict of Interest

The authors declare no conflict of interest.

Data Availability Statement

The data that support the findings of this study are available from the corresponding author upon reasonable request.

Keywords

ablation of metallic nanoislands, gold, kinetic sputtering, potential sputtering, nanoislands, slow highly charged ions

Received: November 22, 2022

Revised: February 15, 2023

Published online: March 22, 2023

- [1] M. A. Nastasi, J. W. Mayer, Y. Wang, *Ion beam analysis: Fundamentals and applications*, CRC Press, Taylor & Francis Group, Boca Raton **2014**.
- [2] I. Utke, S. Moshkalev, P. Russell, *Nanofabrication Using Focused Ion and Electron Beams: Principles and Applications*, Oxford University Press, USA, Cary **2012**, oCLC: 1058352920.
- [3] A. Arnau, F. Aumayr, P. Echenique, M. Grether, W. Heiland, J. Limburger, R. Morgenstern, P. Roncin, S. Schippers, R. Schuch, N. Stolterfoht, P. Varga, T. Zouros, H. Winter, *Surf. Sci. Rep.* **1997**, *27*, 113.
- [4] R. A. Wilhelm, A. S. El-Said, F. Krok, R. Heller, E. Gruber, F. Aumayr, S. Facsko, *Prog. Surf. Sci.* **2015**, *90*, 377.
- [5] R. Heller, S. Facsko, R. A. Wilhelm, W. Möller, *Phys. Rev. Lett.* **2008**, *101*, 096102.
- [6] J. Schweska, H. Inani, M. Tripathi, A. Niggas, N. McEvoy, F. Libisch, F. Aumayr, J. Kotakoski, R. A. Wilhelm, *ACS Nano* **2020**, *8*, 10536.
- [7] R. A. Wilhelm, *Surf. Sci. Rep.* **2022**, *77*, 100577.
- [8] A. El-Said, R. Heller, R. Wilhelm, S. Facsko, F. Aumayr, *Appl. Surf. Sci.* **2014**, *310*, 169.
- [9] A. S. El-Said, R. Heller, W. Meissl, R. Ritter, S. Facsko, C. Lemell, B. Solleder, I. C. Gebeshuber, G. Betz, M. Toulemonde, W. Möller, J. Burgdörfer, F. Aumayr, *Phys. Rev. Lett.* **2008**, *100*, 237601.
- [10] A. S. El-Said, R. A. Wilhelm, R. Heller, M. Sorokin, S. Facsko, F. Aumayr, *Phys. Rev. Lett.* **2016**, *117*, 126101.
- [11] R. Kozubek, M. Tripathi, M. Ghorbani-Asl, S. Kretschmer, L. Madauß, E. Pollmann, M. O'Brien, N. McEvoy, U. Ludacka, T. Susi, G. Duesberg, R. Wilhelm, A. Krashennikov, J. Kotakoski, M. Schleberger, *J. Phys. Chem.* **2019**, *10*, 904.
- [12] C. Länger, P. Ernst, M. Bender, D. Severin, C. Trautmann, M. Schleberger, M. Dürr, *New J. Phys.* **2021**, *23*, 093037.
- [13] J. M. Pomeroy, A. C. Perrella, H. Grube, J. D. Gillaspay, *Phys. Rev. B* **2007**, *75*, 241409.
- [14] S. E. Donnelly, R. C. Birtcher, *Philos. Mag. A* **1999**, *79*, 133.
- [15] E. Gruber, R. A. Wilhelm, R. Pétuya, V. Smejkal, R. Kozubek, A. Hierzenberger, B. C. Bayer, I. Aldazabal, A. K. Kazansky, F. Libisch, A. Krashennikov, M. Schleberger, S. Facsko, A. G. Borisov, A. Arnau, F. Aumayr, *Nat. Commun.* **2016**, *7*, 13948.
- [16] S. Das, A. Sebastian, E. Pop, C. J. McClellan, A. D. Franklin, T. Grasser, T. Knobloch, Y. Illarionov, A. V. Penumatcha, J. Appenzeller, Z. Chen, W. Zhu, I. Asselberghs, L.-J. Li, U. E. Avci, N. Bat, T. D. Anthopoulos, R. Singh, *Nat. Elec.* **2021**, *4*, 786.
- [17] Y. Liu, X. Duan, H.-J. Shin, S. Park, Y. Huang, X. Duan, *Nature* **2021**, *591*, 43.
- [18] S. Choupanian, W. Möller, M. Seyring, C. Ronning, *Nano Res.* **2022**, *16*, 1522.
- [19] S. Choupanian, A. Nagel, W. Möller, C. Pacholski, C. Ronning, *Nanotechnology* **2021**, *33*, 035703.
- [20] A. George, C. Neumann, D. Kaiser, R. Mupparapu, T. Lehnert, U. Hübner, Z. Tang, A. Winter, U. Kaiser, I. Staude, A. Turchanin, *J. Phys. Mater.* **2019**, *2*, 016001.
- [21] F. Trillitzsch, R. Guerra, A. Janas, N. Manini, F. Krok, E. Gnecco, *Phys. Rev. B* **2018**, *98*, 165417.
- [22] C. Monachon, L. Weber, C. Dames, *Annu. Rev. Mater. Res.* **2016**, *46*, 433.
- [23] F. Gołak, P. Mazur, Z. Ryszka, S. Zuber, *Appl. Surf. Sci.* **2014**, *304*, 11.
- [24] J. Shen, D. Zhang, F.-H. Zhang, Y. Gan, *Appl. Surf. Sci.* **2017**, *422*, 482.
- [25] J. Hopster, R. Kozubek, J. Kraemer, V. Sokolovsky, M. Schleberger, *Nucl. Instrum. Meth. B* **2013**, *317*, 165.
- [26] D. Kost, S. Facsko, W. Möller, R. Hellhammer, N. Stolterfoht, *Phys. Rev. Lett.* **2007**, *98*, 225503.
- [27] G. Rizza, P. E. Coulon, V. Khomenkov, C. Dufour, I. Monnet, M. Toulemonde, S. Perruchas, T. Gacoin, D. Maily, X. Lafosse, C. Ulysse, E. A. Dawi, *Phys. Rev. B* **2012**, *86*, 035450.

- [28] C. Dufour, V. Khomenkov, G. Rizza, M. Toulemonde, *J. Phys. D* **2012**, *45*, 065302.
- [29] R. Prasher, *Appl. Phys. Lett.* **2009**, *94*, 041905.
- [30] X. Zhang, D. Sun, Y. Li, G.-H. Lee, X. Cui, D. Chenet, Y. You, T. F. Heinz, J. C. Hone, *ACS Appl. Mater.* **2015**, *7*, 25923.
- [31] Y. U. Staechelin, D. Hoeing, F. Schulz, H. Lange, *ACS Photonics* **2021**, *8*, 752.
- [32] W. Eckstein, R. Dohmen, A. Mutzke, R. Schneider, *SDTrimSP 2007, IPP-reports*.
- [33] A. Mutzke, R. Schneider, W. Eckstein, R. Dohmen, *SDTrimSP Version 5.00 2011, IPP-reports*.
- [34] U. von Toussaint, A. Mutzke, A. Manhard, *Physica Scripta* **2017**, *T170*, 014056.
- [35] L. Sandoval, H. M. Urbassek, *Nanoscale Res. Lett.* **2015**, *10*, 314.
- [36] M. L. Nietiadi, L. Sandoval, H. M. Urbassek, W. Möller, *Phys. Rev. B* **2014**, *90*, 045417.
- [37] X. Wang, Y. Liu, Z. Xu, *Radiat. Phys. Chem.* **2022**, *201*, 110455.
- [38] S. E. Donnelly, R. C. Birtcher, *Phys. Rev. B* **1997**, *56*, 13599.
- [39] R. C. Birtcher, S. E. Donnelly, *Phys. Rev. Lett.* **1996**, *77*, 4374.
- [40] J. Biersack, *Nucl. Instr. and Meth. B* **1993**, *80-81*, 12.
- [41] T. Schenkel, M. A. Briere, A. V. Barnes, A. V. Hamza, K. Bethge, H. Schmidt-Böcking, D. H. Schneider, *Phys. Rev. Lett.* **1997**, *79*, 2030.
- [42] R. A. Wilhelm, E. Gruber, R. Ritter, R. Heller, S. Facsko, F. Aumayr, *Phys. Rev. Lett.* **2014**, *112*, 153201.
- [43] R. A. Wilhelm, E. Gruber, V. Smejkal, S. Facsko, F. Aumayr, *Phys. Rev. A* **2016**, *93*, 052708.
- [44] A. Niggas, J. Schwestka, K. Balzer, D. Weichselbaum, N. Schlünzen, R. Heller, S. Creutzburg, H. Inani, M. Tripathi, C. Speckmann, N. McEvoy, T. Susi, J. Kotakoski, Z. Gan, A. George, A. Turchanin, M. Bonitz, F. Aumayr, R. A. Wilhelm, *Phys. Rev. Lett.* **2022**, *129*, 086802.
- [45] R. A. Wilhelm, W. Möller, *Phys. Rev. A* **2016**, *93*, 052709.
- [46] I. Stabrawa, D. Banaś, A. Kubala-Kukuś, K. Szary, J. Braziewicz, J. Czub, Jabłoński, P. Jagodziński, D. Sobota, M. Pajek, K. Skrzypiec, E. Mendyk, M. Teodorczyk, *Nucl. Instrum. Meth. B* **2017**, *408*, 235.
- [47] J. Burgdörfer, P. Lerner, F. W. Meyer, *Phys. Rev. A* **1991**, *44*, 5674.
- [48] A. Niggas, S. Creutzburg, J. Schwestka, B. Wöckinger, T. Gupta, P. L. Grande, D. Eder, J. P. Marques, B. C. Bayer, F. Aumayr, R. Bennett, R. A. Wilhelm, *Commun. Phys.* **2021**, *4*, 180.
- [49] E. Gnecco, A. Janas, B. R. Jany, A. George, A. Turchanin, G. Cempura, A. Kruk, M. Tripathi, F. Lee, A. Dalton, F. Krok, *Appl. Surf. Sci.* **2023**, *616*, 156483.
- [50] D. Nečas, P. Klapetek, *Open Physics* **2012**, *10*, 1.
- [51] J. Schwestka, D. Melinc, R. Heller, A. Niggas, L. Leonhartsberger, H. Winter, S. Facsko, F. Aumayr, R. A. Wilhelm, *Rev. Sci. Instrum.* **2018**, *89*, 085101.
- [52] A. Niggas, J. Schwestka, D. Weichselbaum, R. Heller, F. Aumayr, R. A. Wilhelm, *Proc. SPIE 12131, Nanophotonics IX, Strasbourg, France*, **2022**, <https://www.spiedigitallibrary.org/conference-proceedings-of-spie/12131/2624402/Coincidence-technique-to-study-ion-induced-electron-emission-from-atomically/10.1117/12.2624402.full>.
- [53] RoentDek Handels GmbH, <http://www.roentdek.com> (accessed: September 2022).